Journal of Porous Materials (2024) 31:1601–1616
https://doi.org/10.1007/s10934-024-01608-6

A 2-dimensional modelling of the coating process of nickel on polyurethane foam via electrodeposition

N. Ghiasi[1] · **F. Kunz**[2] · **A. Jung**[2] · **S. Diebels**[1]

Accepted: 2 April 2024

Abstract

A numerical model is proposed to investigate the electrodeposition coating process of open-porous polyurethane (PU) foams with nickel. The modelling approach is based on the mixture theory, which accounts for the multi-phase nature of the system comprising the porous foam structure and the electrolyte which consists of the deposition material in form of cations. The model takes into consideration various physical and electrochemical phenomena, including different ionic transport mechanisms, i.e. diffusion, convection and migration. By solving the governing equations numerically, the coating process and the relevant variables are predicted over time. The simulation results are compared with experimental data to assess the agreement between the model and the experimental results. The findings reveal that the numerical model provides valuable insights into the electrodeposition process and facilitates a deeper understanding of the underlying mechanisms and it can be used for optimizing the coating process parameters.

Keywords Hybrid metal foams · Ni/PU foams · Double-sided modelling · Mixture theory · Coupled problem · Parameter identification

1 Introduction

The study of mass transport and reaction of fluids in natural and synthetic porous media is an interesting research topic encountered in a wide range of engineering and industrial problems, from oil extraction and petroleum industry to the chemical processes involving catalysts, development of electrodes and batteries [1, 2].

Porous materials are a class of materials typically characterized by their unique structures and properties, such as pore size distribution, internal surface area, and comprising material. Due to their potential to deal with various technological challenges, these materials are suitable for specific applications, including energy storage and insulation, filters, and biomedical implants [3–5]. However, their application is often limited by their poor mechanical strength, stability, and bio-compatibility. As a result, the field of porous materials research has been rapidly growing and advancing. Metal coating via electrodeposition offers a solution to some of these challenges by creating a conformal coating on the surface of the open-cell porous foam, commonly known as hybrid metal foams, which can improve the mechanical and geometrical properties of the original substrate material [6].

Electrodeposition, also known as electroplating, is a process in which a metal ion is reduced and deposited onto a conductive surface to form a thin layer of metal. Hence, the first step in the coating of porous polymer foams is to make them electrically conductive. This is achieved by dip-coating the foams in a conductive graphite lacquer. In the next step, this dip-coated foam is connected to the cathode and exposed to the flow of an electrolyte, which contains the metal ions to be deposited. By applying an electric current, which is passed through the electrolyte and the conductive surface, the positively charged metal ions (cations) are attracted to the negatively charged conductive surface (cathode) and are reduced to solid metal, forming a thin layer of metal coating [7–9]. The thickness and quality of the coating can be controlled by adjusting the electric current, the

---

A. Jung
junga@hsu-hh.de

S. Diebels
s.diebels@mx.uni-saarland.de

[1] Applied Mechanics, Saarland University, Campus A4 2, Saarbrücken 66123, Saarland, Germany

[2] Protective Systems, Helmut-Schmidt University/University of the Federal Armed Forces Hamburg, Holstenhofweg 85, Hamburg 22043, Germany

flow of electrolyte, the concentration of the metal ions in the electrolyte, and the duration of the process. Comprehensive studies on the production of hybrid foams via electrodeposition have been carried out by Jung et al. [6, 9–12] and they improved the coating process significantly compared to the former studies by Bouwhuis et al. [13], Boonyongmaneerat et al. [14] and Sun et al. [15–17]. Jung et al. investigated the metal coating of metallic and polymeric substrates and compared their mechanical properties with each other as well as their own properties before and after coating. However, the surface modification of open-cell foams using this coating technique is often challenging due to the complex geometries and large internal surface areas of these materials [7, 10]. Furthermore, the mass transport limitations [18–20] lead to a non-homogeneous coating thickness which affects the efficiency of such hybrid foams.

To overcome these limitations, modelling and simulation techniques have been developed to study and optimize this process. In this context, simulation offers a powerful tool to investigate the underlying mechanisms and optimize the coating controlling parameters for an improved performance. Moreover, understanding of the flow behaviour through porous materials is of great importance to be able to expand their applications and develop new efficient an sustainable materials.

The mass transport through the open-cell foam in an electrodeposition process is governed by a highly non-linear coupled system. The flow through the pores is controlled by multiple mechanisms: the convection of the fluid is realised by a pump, which produces a pressure gradient; the migration of the ions is realised by an electrical current, which is produced by an electrical potential gradient; and the diffusion of ions is realised by different ion concentration at the inlet and outlet of the foam. Furthermore, by the deposition of ions on the struts and the foam's geometrical evolution, an additional sink term for the ions is introduced which complicates the problem further [8, 21].

In order to get a better perception of the electrodeposition process and a general understanding of flow behaviour inside the porous medium, the first necessary step is to develop a quantitative model at the macro scale. This model should be built in such a way that takes into account all the main transport mechanisms as well as the multi-phase nature of the process. In this regard, mixture theory grants an appropriate mathematical framework to deal with such complex problems.

Mixture theory is a branch of continuum mechanics used to describe and analyse the behaviour of heterogeneous materials which are made up of multiple constituents or phases, each with their own distinct properties and behaviour that affect the overall behaviour and deformation of the material. The main idea is to consider the entire system as superimposed continua and to deal with each phase as a separate continuum with its own governing equations. These equations take into account the interactions between the constituents, such as exchange of mass, momentum, and energy. Hence, the overall behaviour of the material is the result of the superposition of individual behaviours of each constituents [22–24]. Mixture theory has been widely used in various fields of engineering, including chemical engineering and materials science and particularly in analyzing complex materials such as porous materials that exhibit non-homogeneous behaviour [23, 25–31] and has proven particularly useful in modelling such problems.

The focus of this study is modelling the coating process of polyurethane foams with nanocrystalline nickel via electrodeposition which leads to the production of Ni/PU hybrid foams. Not only have these hybrid foams lightweight features of highly porous solids and an increased strength due to nickel coating but they also are economical in comparison to similar metal foams [10]. However, some difficulties emerge during the production of Ni/PU foams such as heterogeneous coating thickness due to mass transport limitations which leads to a heterogeneous distribution of the mechanical properties. To improve the production procedure, leveraging the results of numerical simulations can be valuable. The proposed model should be able to describe the flow behaviour within the electrodeposition process precisely and yet be as simple as possible. Modelling the coating of porous materials has been the subject of interest in a few studies in recent years. The coating process of open-cell foams and specifically the electrodeposition process of nickel ions on polyurethane foams have been numerically simulated by Grill et al. [8, 32, 33] in which they investigated the influence of electrodeposition parameters on the coating thickness homogeneity and compared the numerical results with the experimental data. Grill et al. used the Nernst-Planck equation to describe a one-sided coupled electrodeposition process with constant geometrical and process parameters. However, a more precise model should take into account the influence of coating on these parameters, e.g. the changes in the permeability due to increasing coating thickness. In a previous work, the authors [21] developed a two-sided coupled model based on the mixture theory on a macroscopic scale, which is able to give a qualitative insight on the properties changes under the influence of coating. In their model, concentration, pressure and electric field can be calculated using a system of three coupled equations. With the help of a back-coupling technique, the changes of properties in each iteration have been taken into account for the calculation of properties in the next iterations.

The purpose of this study is to evolve the suggested one-dimensional model in [21] further for a two-dimensional domain. Moreover, by calculation of the local electrical current using the Butler–Volmer equation [34–36], the thickness of deposition can be estimated from Faraday's law [34, 37]. Subsequently, the numerical results will be compared with the experimental results to evaluate the performance and efficiency of the proposed model.

In the next section, the electrodeposition method and the experiment’s conditions are described in details. In the third section, the mathematical model and the governing equations that describe the process, are presented. They will be numerically solved using a finite difference method. A problem based on the experiment’s initial and boundary conditions will be defined in Sect. 4 and the numerical and experimental results will be compared with each other to validate the model. Finally, a summary of the obtained results and conclusions is given in the last section of this study.

2 Experimental part: hybrid foam production and characterization

2.1 Materials and methods

The electrodeposition process takes place in a galvanic reactor, where the anodes as well as the cathode are placed in an aqueous nickel sulfamate electrolyte. To guarantee a maximum ion concentration during the deposition process, a flow of electrolyte through the open-porous foam placed in the reactor is generated by a membrane pump. A cartridge filter with a pore size of 10 μm removes contamination from the inflowing electrolyte before it reaches the reactor. During the complete deposition process, the electrolyte is additionally stirred and kept on a constant temperature level of 50 °C. The schematic arrangement of the heating- and stirring-unit, the filtration- and circulation-unit, as well as the power supply by the galvanostate is schematically shown in Fig. 1a.

The flow reactor consists of five modules as shown in Fig. 1b. Starting from the bottom, the first module (inlet module) contains the inlet valve for the electrolyte, which is pumped in and generates the inflow. The second and the fourth modules are respectively the lower and upper anodes, which carry nickel for the dissolving process during deposition. Both anodes consist of two layers of titanium stretch metal, filled with spherical, s-polarized nickel pellets, which dissolve during the galvanic-driven oxidation process to nickel ions and drive the mass transport. To protect the electrolyte from coarse contamination by sludge during dissolution, the anodes are covered with a layer of non-woven fabric. The electrical contact between the two anodes and the power supply is established via an insulated titanium connection leading through the reactor wall to the outside. The third module, the cathode, is placed in the middle of the reactor between both anodes and is marked as foam cathode. This module contains the pre-treated, carbon coated PU foam, which is also connected via four insulated cables to the cathodic pole of the power supply. The fifth module (outlet module) contains the outlet valve and is directly connected to the heating- and stirring unit, so the electrolyte can be reheated and stirred again in the exchange vessel for further pumping through the reactor.

PU foams (Schaumstoff Direkt Rüdiger Nolte, Enger, Germany) with a pore size of approximately 10 ppi (pores per inch) were used as a precursor material for the galvanic coating process. The specimen was cut into a cylindrical, disc-like form by an electric hot wire to a resulting diameter of 210 mm and a thickness of 40 mm. To produce a

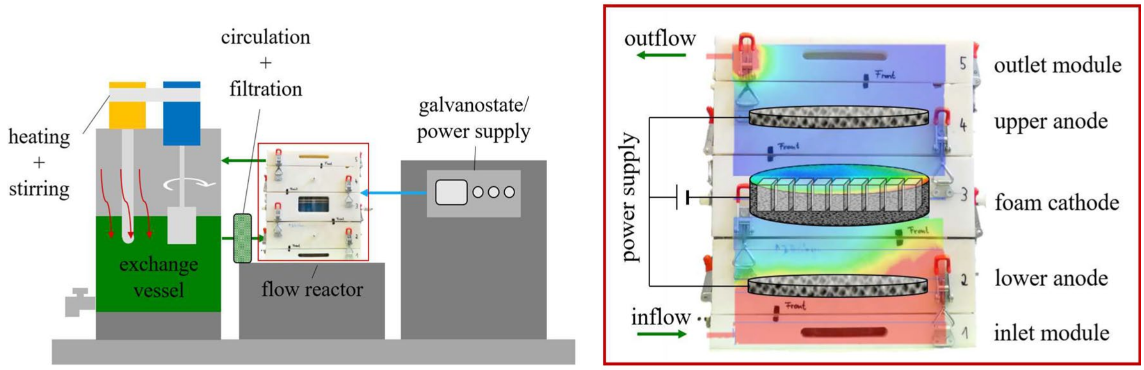

(a) (b)

Fig. 1 **a** The arrangement of the exchange vessel, where the electrolyte is continuously stirred and kept on a constant level of temperature, the pumping and filtration unit to generate a constant electrolyte flow and the galvanostate, which acts as the power supply to drive the electrodeposition. The connection to the flow reactor is schematically shown. **b** The flow reactor with its schematic arrangement of the two nickel anodes and the open-cell foam cathode, which is placed between both anodes in the center of the reactor. A schematic, qualitative flow velocity distribution of the reactor cross-section together with a corresponding density distribution on the foam surface, is overlaid (red: high flow velocity/density, blue: low flow velocity/density) (Color figure online) conductive surface on the polymer foam, a pre-treatment step is necessary. Therefore, the precursor material is dipped into a graphite conductive lacquer (Graphit 33, CRC Kontakt Chemie, Iffezheim, Germany) twice. For a coating homogenization of the applied graphite layer after two dip-coatings and the removal of superfluous varnish, the samples were dried for 10 min under a constant air pressure.

The carbon-coated, conductive foam substrate was connected to the cathodic pole of the power supply with four stranded wires. After assembling the reactor and filling it with electrolyte, a constant volume flow of 4 $\mathrm{l/min^{-1}}$ was set. By applying a current density of 1.65 $\mathrm{mA\ cm^{-2}}$, the electrodeposition process was started and carried out for 108.5 h. A high distance between both anodes and the cathode facilitates an early calming of the flow-induced turbulences, so that the electrolyte flow dominates in the thickness direction through the foam.

The deposition parameters for the production of the hybrid metal foam were selected according to Kunz et al. [7]. They result from the maximum degree of homogeneity, as well as the highest reduced overcoating tendency, that was achieved by an optimized flow velocity and anode distance. The exact optimization process can be found by Kunz et al. [7]. The introduction of an electric voltage and the corresponding current promotes the deposition process of nickel ions on the cathode surface.

2.2 Coating thickness distribution analysis

The produced hybrid metal foam shows a layer of nickel coated on every stochastically distributed strut in the total volume. The coating thickness seems to vary depending on the position in the foam volume. To characterize the coating distribution on the struts in the whole hybrid metal foam, it is necessary to analyze the coating thickness with different methods on different scales. First, the global distribution of the deposited mass of nickel is taken into account. Therefore, the hybrid metal foam was cut into cuboid specimens with a size of 20 × 20 × 40 mm by a band saw (Fig. 2). The global distribution of the mass of coated nickel can be described by the density factor *df*, which is known as the percentage value of the specific density of one cuboid specimen $\rho_{specimen}$ divided by averaged specific density of all analyzed cuboid specimens $\rho_{average}$ cut out of the total hybrid metal foam plate. The specific density describes the mass of porous media compared to its volume including free pore space. In a further study of Kunz et al. [7] it was found, that the local coating thickness shows an inhomogeneous distribution over the foam height. Therefore, it is necessary to take the height-dependent coating thickness distribution in the cuboid specimens into account. It is characterized by panoramic microscopy using a light microscope. The surface of the cross-section was metallographically prepared by grinding until a particle size of approx. 15.3 ± 1 μm. An optical light microscope (VHX-7000 Digital Microscope, Keyence, Neu-Isenburg, Germany) was used in combination with a standard objective lense (VH-Z20R 20-200, Keyence, Neu-Isenburg, Germany) and a magnification of 50. The software provided by the producer allows a panoramic image acquisition of the complete cross-section surface of each specimen prepared out of the foam plate. The local coating thickness of the stochastic distributed struts was measured by the ImageJ® based open source program Fiji®. The measured values have been categorized by their position. For the estimation of overcoating tendencies at the outer areas of the cross-section, the local coating values have been averaged over three areas (bottom, center and top) of the foam, as shown in Fig. 2 corresponding to Kunz et al. [7], so the impact of electrolyte flow, anode distance and intrinsic physical properties can be estimated.

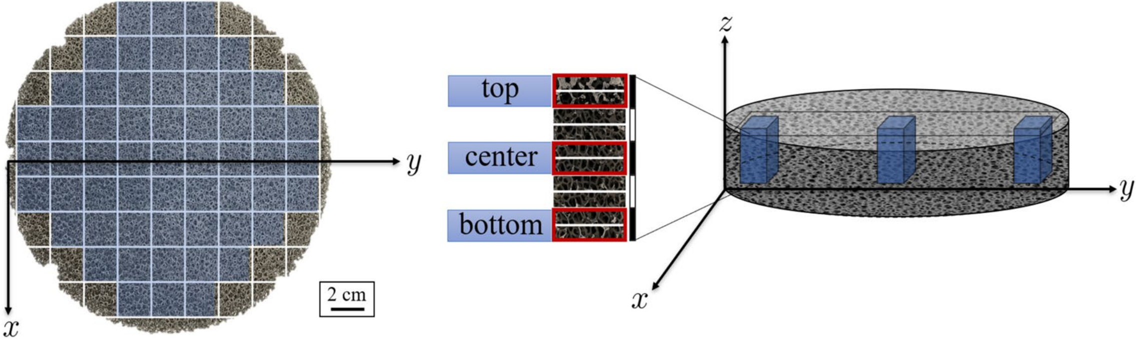

Fig. 2 Cuboid specimens cut out of the disc-like foam specimen and the analyzed top, center and bottom domains (Color figure online)

3 Numerical part: mathematical model

To obtain a numerical representation of the mentioned electrodeposition process in the previous section, it is important to choose a method that can depict the highly coupled governing interactions between different phases of the problem. Mixture theory [22, 23, 31, 38] offers a simplified and yet comprehensive framework to model the flow through porous materials. By this means, the electrodeposition process of nickel ions on polyurethane foams can be represented as a three-phase model, as shown in Fig. 3. In this model, the representative volume element (RVE) at the macroscopic spatial position $\mathbf{x}$ is made up of a fluid phase (the electrolyte), φ^f, consisting of water, φ^w, and nickel ions, φ^{ni}, flowing through a solid phase (PU foam), φ^s.

For convenience, the other constituents of the electrolyte are neglected. Based on the concepts of mixture theory, e.g. Trussdell [24] and Bowen [22], different physical properties can be specified for each constituent occupying the same macroscopic position and for the whole mixture at that position.

After defining the kinematics, the balance equations and the appropriate production terms should be defined for each constituents to take into account the interphasial interactions. However, according to the mass conservation principal, the deposited mass on the solid phase is equal to the reduced mass of the fluid phase. Therefore, for the sake of simplicity, the RVE under observation can be reduced to a 2-phase continuum of the pore fluid (water + nickel) while the effect of solid phase on the fluid is considered only through the interaction forces. This reduction is possible if the solid foam structure is assumed to be rigid. The last step is to define the suitable constitutive equations for the flux term, the mass supply and the fluid's density to obtain the final closed equation set. Ghiasi et al. [21] provided a detailed comprehensive description on the necessary kinematics and the derivation of the governing equations. For the sake of brevity, it is refrained to go into all the details again in this study and the explanations here are limited only to the main equations [21].

The model is obtained from the mass balance equations of the fluid and the nickel ions alongside the application of Darcy's law [39–41]. A simplified Newtonian, laminar flow through the open-porous foam is assumed. The influence of any experimentally observed local turbulence in the flow will be considered through the choice of boundary conditions. The simplified model consists of three coupled partial differential equations for the distribution of concentration of ions c, pressure p, and electric field $\mathbf{E}$, within the foam [21].

$$\begin{aligned}\frac{\partial c}{\partial t} = \frac{1}{\rho_0 + A_2 c + A_3(p-p_0)}\Big[&\underbrace{A_1 c(1-c)}_{\text{Sink}} + \underbrace{D\mathrm{div}(\mathrm{grad}c)}_{\text{Diffusion}}\\ &+ \underbrace{\frac{zFD}{R\theta}(\mathrm{grad}c\cdot\mathrm{grad}\phi + c\ \mathrm{div}(\mathrm{grad}\phi))}_{\text{Migration}}\Big]\\ &+ \underbrace{\frac{1}{K}\big(n^f\mathrm{grad}p - (\rho_0 + A_2 c + A_3(p-p_0))\mathbf{g}\big)\cdot\mathrm{grad}c}_{\text{Convection}}\end{aligned} \tag{1}$$

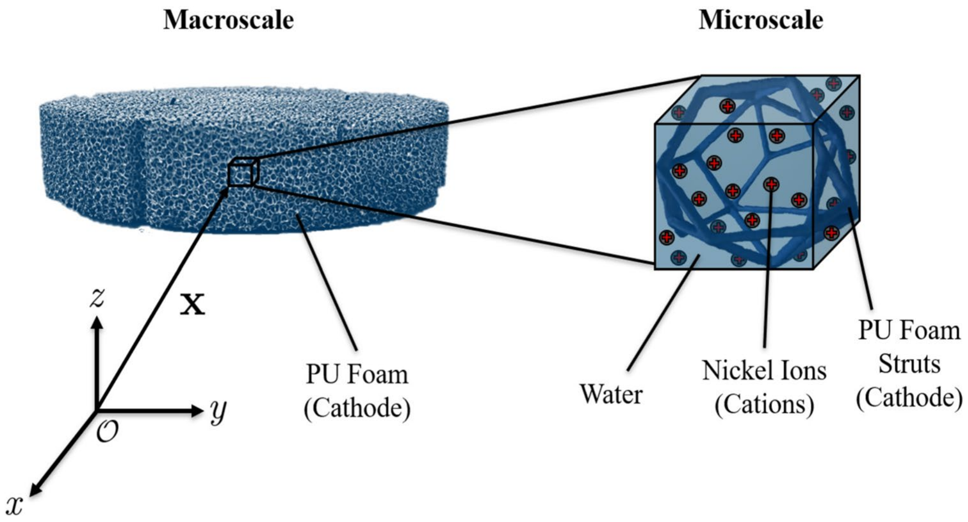

Fig. 3 Schematic representation of the problem as a 3-phase mixture consisting of the solid phase saturated by water and ions. A material point on the macroscale can be resolved on the microscale by an RVE

$$
\begin{aligned}
\frac{\partial p}{\partial t} = \frac{1}{A_3}\Bigg[& \left(A_1 c\right)\left(1 - \frac{A_2}{\rho_0 + A_2 c + A_3(p - p_0)}(1 - c)\right) \\
& - \frac{A_2 D}{\rho_0 + A_2 c + A_3(p - p_0)} \\
& \left[\mathrm{div}(\mathrm{grad}c) + \frac{zF}{R\theta}(\mathrm{grad}c \cdot \mathrm{grad}\phi + c\ \mathrm{div}(\mathrm{grad}\phi))\right] \\
& + \frac{\rho_0 + A_2 c + A_3(p - p_0)}{K} \\
& \left[n^f \mathrm{div}(\mathrm{grad}p) - \mathbf{g} \cdot (A_2 \mathrm{grad}c + A_3 \mathrm{grad}p)\right] \\
& + \frac{A_3}{K}(n^f (\mathrm{grad}p)^2 \\
& - \left(\rho_0 + A_2 c + A_3(p - p_0)\right)\mathbf{g} \cdot \mathrm{grad}p)\Bigg]
\end{aligned} \tag{2}
$$

$$
\frac{\partial \mathbf{E}}{\partial t} = \frac{\mathbf{I}_{ext}}{\epsilon} - \frac{Fz\mathbf{J}}{\epsilon} \tag{3}
$$

Equation (3) is the electrical displacement–current equation describing the temporal change of the electric field [42, 43]. The flux term **J** is expressed by the Nernst–Planck equation:

$$
\mathbf{J} = c^*\mathbf{v} - D\ \mathrm{grad}c^* - \frac{zF}{R\theta}Dc^*\ \mathrm{grad}\phi \tag{4}
$$

where:

$$
c^* = \frac{c\rho^f}{MW^{ni}} \tag{5}
$$

Finally, the electric field is related to the electrical potential as:

$$
\mathbf{E} = -\mathrm{grad}\phi \tag{6}
$$

which is the required term in Eqs. (1) and (2).

The symbols being used in Eqs. (1)–(6) are listed in Table 1.

The coefficients A_1, A_2 and A_3 are unknown parameters that must be identified through inverse estimation [21]. These coefficients were introduced during the definition of constitutive equations for the production term and the fluid density. A_1 is the proportionality coefficient that relates the sink to the available ion concentration. A_2 and A_3 relate the fluid density to the concentration and pressure, respectively [21].

3.1 Coating thickness calculation

Based on Faraday's law of electrolysis [37, 44], the amount of deposition on an electrode is directly proportional to the electrical charge Q (C). This statement can be defined in terms of moles of reduced metal, M (mol), via charge, as follows:

Table 1 Symbols' glossary

Symbol	Name	Unit
c	Mass concentration of nickel ions	1
c^*	Mass concentration of nickel ions	$\mathrm{mol/m^3}$
p	Pressure	Pa
ρ_0	Density of pure water	$\mathrm{kg/m^3}$
p_0	Reference pressure	Pa
D	Diffusion coefficient	kg/m s
K	Drag coefficient	$\mathrm{kg/m^3\ s}$
n^f	Porosity	1
$\mathbf{g}$	External body force	$\mathrm{m/s^2}$
t	Time	s
$\mathbf{E}$	Electric field	V/m
z	Electric charge of the ions	1
F	Faraday constant	C/mol
R	Universal gas constant	N m/ K mol
θ	Absolute temperature	K
ϕ	Electrical potential	V
$\mathbf{I}_{ext}$	External current density	$\mathrm{A/m^2}$
ϵ	Absolute permittivity	$\mathrm{C^2/N\,m^2}$
$\mathbf{J}$	Flux of ions	$\mathrm{mol/m^2\ s}$
$\mathbf{v}$	Fluid mean barycentric velocity	m/s
MW^{ni}	Molar weight of nickel	kg/mol
ρ^f	Fluid partial density	$\mathrm{kg/m^3}$

$$
M = \frac{Q}{zF} \tag{7}
$$

Using the definition of molar weight of nickel (MW^{ni}), the deposition mass, m (kg), can be obtained from the molar mass of deposition, according to:

$$
m = MW^{ni}\ M \tag{8}
$$

Moreover, to obtain the amount of total charge being used over the deposition process, the integral of the electrical current, $I(\mathbf{x}, t)$ (A), during the deposition time should be calculated.

$$
Q = \int I(\mathbf{x}, t)dt \tag{9}
$$

According to the definition of density, the coating thickness $\delta(\mathbf{x}, t)$ can be defined in terms of deposition mass m (kg) as:

$$
\delta(\mathbf{x}, t) = \frac{m}{\rho^{ni}A} \tag{10}
$$

where ρ^{ni} is the density of nickel and A is the area of deposition, i.e. the internal surface of the foam. Substituting Eqs.

(8) and (9) in Eq. (7), and then using the result in Eq. (10), the coating thickness can be computed.

$$\delta(\mathbf{x},t) = \frac{MW^{ni}\int I(\mathbf{x},t)dt}{zF\rho^{ni}A} \tag{11}$$

Taking a glance at Eq. (11), it can be noticed that the local coating thickness at any time t is proportional to the integral of local electric current at that time. The Butler–Volmer equation [34, 35, 44] gives a comprehensive insight in the formulation of electrode kinetics and makes it possible to calculate the local current density, I/A (A/m^2), as a function of ion concentration.

$$\frac{I(\mathbf{x},t)}{A} = I_{ext}\left[\frac{c(\mathbf{x},t)}{C_\infty}\exp\left(\frac{\alpha_A zF\eta}{R\theta}\right) - \exp\left(\frac{-\alpha_C zF\eta}{R\theta}\right)\right] \tag{12}$$

where C_∞ is the initial reference concentration, α_A and α_C are the anodic and cathodic charge transfer coefficients, and η denotes the overpotential [35, 36, 45].

3.2 Back-coupling technique

Equations (1)–(3) contain geometrical parameters which start to change with the start of the coating process. These structural changes have a direct effect on the other process parameters such as fluid velocity or pressure distribution. To obtain a more precise model, it is important to consider the updated values of the structural parameters for the calculations in the next time steps. Ghiasi et al. [21] developed a simplified model to perform back-coupling calculations.

In this model, the struts are considered as simple cylinders and the initial radius of these struts is calculated from the solidity,

$$n^s = 1 - n^f, \tag{13}$$

as

$$n^s(\mathbf{x},1) = \frac{dv^s(\mathbf{x},1)}{dV^{el}} \tag{14}$$

where dV^{el} is the total volume of each volume element containing one strut and dv^s is the volume of the strut inside each volume element [21].

By calculating the coating thickness in each temporal interval from Eq. (11), the new radius, the new solidity, and therefore the new porosity can be calculated. In their model, they used the updated porosity to obtain the new permeability. Hommel et al. [46] provided a detailed review study about the numerous practical porosity-permeability relations suggested in various literature. The following relation has been chosen from [46] to calculate the new permeability.

$$\frac{K}{K_0} = \left(\frac{n^f}{n^f_0}\right)^\beta \tag{15}$$

The exponent β in this equation is an empirical parameter [46], which depends on the local topology of the foam and has to be determined from experiments.

3.3 Numerical implementation: finite difference method

Due to the complexity and high non-linear nature of the system of coupled Eqs. (1)–(3), choosing a proper method among the available numerical methods is greatly limited. Finite difference method (FDM) [47–50] is a valuable asset which offers a very simple and straight-forward approach to deal with such non-linear partial differential equations (PDE), especially for geometrical simple domains.

Following the solution procedure in [21], the equations are discretized explicitly, which avoids the time-consuming, coupled treatment of the non-linear set of equations. Benefiting from different schemes offered by FDM, the time derivatives and second order spatial derivatives are discretized by a forward and a central scheme, respectively. An upwind discretization scheme (one-sided differences) is useful to treat the convection and migration terms, to be able to take into account the direction of flow and electrical filed, respectively. The detailed arguments are presented in [21].

In this study an additional predictor–corrector method is also used to modify the computation by using a weighted average of old and computed values. This approach is a two-step process that combines a predictor step and a corrector step. It's commonly used in time-dependent problems where iterative refinement of the solution is desired to achieve accurate results. In the predictor step, an initial estimate of the solution at the next time or spatial step is computed based on the current state of the solution and the governing equations. This step is often simpler and faster but may introduce some errors. Then this predicted solution is used as an intermediate solution, and additional correction terms are calculated. These correction terms are typically based on the residual errors introduced in the predictor step. The corrector step aims to refine the solution and improve accuracy.

4 Results and discussion

To have a better perspective on the performance of the model, the experimental results are presented and compared with the equivalent numerical results.

To investigate the problem numerically it is important to reduce the number of parameters by assuming the process as simple as possible. Moreover, due to the large disparity between real time and space domain ranges, divergence and stability issues can arise. In this case normalizing can help balance the discretization and improve the accuracy of simulation. Hence, inspired by the previous study [21], by suitable substitutions of variables and characteristic numbers, temporal and spatial domains, as well as the process variables are normalized. Therefore, the problem is modeled on a square computational domain with a length of 1, in $y - z$ plane in the middle of the foam, as shown in Fig. 4. The square numerical domain has been scaled according to the lengths of the sample rectangular domain.

As mentioned in Sect. 2, the investigated domains for the experimental results are cuboid specimens with the size of $20 \times 20 \times 40$ mm, being cut from the cylindrical foam with the diameter of 210 mm (see Fig. 2). Hence, the experimental results are demonstrated in the respective regions. For the numerical modelling, the respective dimensions and positions are specified on the normalized domain accordingly.

4.1 Numerical model conditions

Considering the problem domain in Fig. 4, the corresponding initial and boundary conditions are defined in such a way to represent the experimental conditions of Kunz et al. [7] and yet be as simple as possible.

Initially, under the absence of any applied pressure or electrical current, the foam is plunged into the electrolyte with a homogeneously distributed infinite ion concentration. Hence, the initial conditions at any point $\mathbf{x} = (y, z)$, are:

$$c(\mathbf{x}, 0) = C_\infty \tag{16}$$

$$p(\mathbf{x}, 0) = p_0 \tag{17}$$

$$E(\mathbf{x}, 0) = E_0 \tag{18}$$

According to the experiment, the process starts when the pump reaches to the designated pressure P_{max} at the inlet. Moreover, taking a glance at Fig. 1b, an inhomogeneous inlet flow velocity can be noted. Hence, based on Darcy's law, the pressure distribution at the inlet of the foam should be inhomogeneous. On the other hand, the lower anode in the experimental setup of Fig. 1 provides an infinite ion reservoir at the inlet. The concentration of the ions at this area is being kept constant via the ion reservoir (anode) and can be described using a Dirichlet type boundary condition. In the simplified model, it is assumed that the electrical field at the inlet of the foam is only affected by the applied external electric current. All in all, the inlet boundary conditions are:

$$c(y, 0, t) = C_\infty \tag{19}$$

$$p(y, 0, t) = (P_{max} - p_0)y \tag{20}$$

$$E(y, 0, t) = E_1 \tag{21}$$

On the outlet of the foam, the ion concentration is influenced both by the flow of electrolyte (the pump), and the upper anode (see Fig. 1). Hence, a Robin boundary condition can be a suitable choice to describe the convection and diffusion effects. Moreover, the pressure reaches the constant outlet pressure p_0. Hence, considering the same argument about the electrical field at the inlet, the boundary conditions at the outlet are:

$$a\, c(y, 1, t) + (1 - a)\, \frac{\partial c(y, 1, t)}{\partial z} = a\, C_\infty \tag{22}$$

$$p(y, 1, t) = p_0 \tag{23}$$

$$E(y, 1, t) = E_1 \tag{24}$$

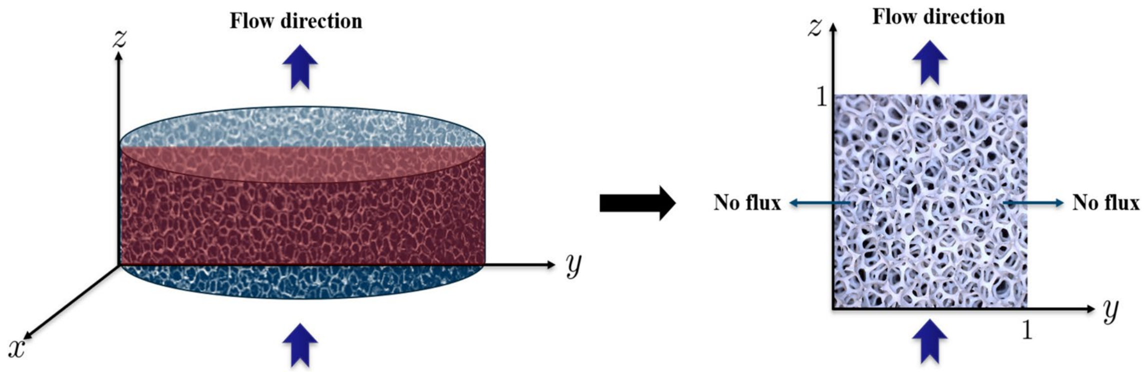

Fig. 4 Normalized 2-dimensional problem domain (red) from the $y - z$ foam's mid-plane (left), with the direction of flow against the gravity (right) (Color figure online)

Table 2 Magnitudes of problem's physical constants

Constant	Value	Constant	Value
ρ_0	$1000\,\mathrm{kg/m^3}$	D	6.8×10^{-10} kg/m s
z	2	F	96485.33 C/mol
R	8.31 Nm/Kmol	θ	323 K
ϵ	70 $\mathrm{C^2/Nm^2}$	I_{ext}	16.5 $\mathrm{A/m^2}$
K	1.3×10^5 $\mathrm{kg/m^3}$ s	n^f	0.9
g_y	0 $\mathrm{m/s^2}$	g_z	$9.8\,\mathrm{m/s^2}$
MW^{ni}	5.87×10^{-2} kg/mol	η	0.2 V
α_A	0.5	α_c	0.5

Table 3 Assumed magnitudes of input parameters

Constant	Value	Constant	Value
A_1	-1×10^2 $\mathrm{kg/m^3s}$	A_2	1.5×10^3 $\mathrm{kg/m^3}$
A_3	2×10^{-1} $\mathrm{s^2/m^2}$	a	9×10^{-1}

The coefficient a in Eq. (22) is the parameter determining the ratio of convection and diffusion influence.

In the simplified model, it is assumed that there will be no flux from the right and left sides of the foam. Hence, a Neumann type boundary condition will be defined for all the variables at both sides:

$$\frac{\partial c(0,z,t)}{\partial z} = \frac{\partial c(1,z,t)}{\partial z} = 0 \tag{25}$$

$$\frac{\partial p(0,z,t)}{\partial z} = \frac{\partial p(1,z,t)}{\partial z} = 0 \tag{26}$$

$$\frac{\partial E(0,z,t)}{\partial z} = \frac{\partial E(1,z,t)}{\partial z} = 0 \tag{27}$$

According to the experimental conditions described in Sect. 2, the process temperature is assumed to be kept constant at 50 °C, and an external current density of 16.5 $\mathrm{A/m^2}$ is applied on a PU foam with 90 percent porosity [7]. The magnitudes of different physical constants in Eqs. (1)–(6) and (12) are listed in Table 2.

The diffusion coefficient D is assumed to be equal to the ionic diffusion coefficient of Ni^{2+} in free water [51]. The values of charge transfer coefficients α_A and α_C are based on the common assumption of symmetric electron transfer in the Butler–Volmer equation [34, 44]. Moreover, for the sake of simplicity and mathematical convenience, the overpotential η is assumed to be constant during the process and its value is chosen heuristically.

The input variables in the problem are chosen according to Ghiasi et al. [21], as listed in Table 3.

According to the constitutive equations defined in [21] and the incompressibility assumption, the effect of pressure change on the electrolyte density is negligible compared to the concentration change. Hence, the pressure constant A_3 must be much smaller than the concentration constant A_2. Also A_1 is a sink constant and therefore must be negative.

The representative normalized time and space ranges and steps are defined as:

$$0 \le t \le 1; \;\; \Delta t = 10^{-3} \tag{28}$$

$$0 \le y \le 1; \;\; \Delta y = 10^{-2} \tag{29}$$

$$0 \le z \le 1; \;\; \Delta z = 10^{-2} \tag{30}$$

The problem can be simplified further by using a single representative coefficient for each transfer mechanism in Eq. (1), as follows [21]:

$$\text{Source term:} \quad \lambda_S = \frac{A_1}{\rho^f} \tag{31}$$

$$\text{Diffusion term:} \quad \lambda_D = \frac{D}{\rho^f} \tag{32}$$

$$\text{Migration term:} \quad \lambda_M = \frac{zFD}{\rho^f R\theta} \tag{33}$$

$$\text{Convection term:} \quad \lambda_C = \frac{1}{K} \tag{34}$$

where ρ^f is the fluid density and defined as a constitutive equation in [21].

In the following, the simulation results using the parameters in Tables 2 and 3 are presented. Moreover, the experimental results are simulated with the proposed model and compared with the respective numerical results.

4.2 Numerical simulation: global results

The responses of the defined problem at the last time step on the considered domain of Fig. 4 are presented in this section.

Figure 5a presents the ion concentration distribution in the foam domain. The concentration of ions is considerably higher at the inlet and outlet of the foam and it reaches to an almost constant value in the central areas. This behaviour has been also reported in the experimental observations [7].

The z-component of the electrical field distribution in the domain is calculated based on Eq. (3) and depicted in Fig. 5b. The experimental analysis of the coating thickness distribution shows significantly increased amounts of nickel in the upper (outlet) and lower (inlet) areas of the foam. The higher coating thicknesses in these areas can be explained by

Fig. 5 *Numerical results:* The 2D distribution of **a** concentration and **b** electrical field (E_z) in the $y-z$ plane

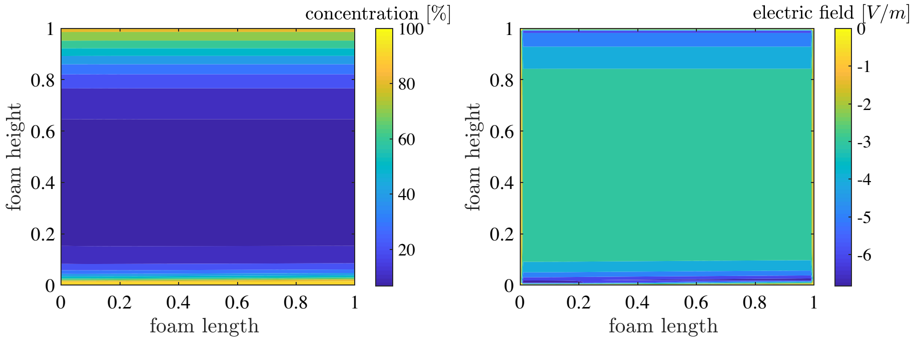

(a)

(b)

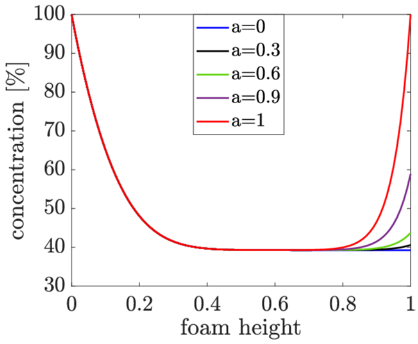

Fig. 6 *Numerical results:* The 1D concentration response at $y = 0.5$ for different values of Robin boundary condition parameter a

a higher ion concentration. The decrease of the concentration towards the foam center can be explained by the reduced mass transport. The decreasing electric field to the foam center is related to the open porous, conductive hybrid foam structure as well as the Faraday law.

The influence of different magnitudes of parameter a in the Robin boundary condition of Eq. (22) on the concentration trend is illustrated in Fig. 6. The values are the considered at the middle of the foam at $y = 0.5$ along the flow direction. The value of parameter a can have a significant impact on the behaviour of the boundary condition and the overall behaviour of the system it describes. As can be seen in Fig. 6, when $a = 0$ the boundary condition simplifies to the Neumann boundary condition. In this case, there is no diffusive flux at the boundary $z = 1$, and the boundary condition is entirely dominated by convection. It represents a situation where there is no mass diffusion across the boundary, and the value of C_∞ controls the rate of convection at the boundary. On the other hand, when $a = 1$ the boundary condition is Dirichlet type. In this case, there is no convection at the boundary $z = 1$, and the boundary condition is entirely dominated by diffusion. It represents a situation where the value of concentration at the boundary is fixed at C_∞ and there is no convective transfer of mass. For any other value of $0 \leq a \leq 1$, the boundary condition is a combination of both diffusion and convection.

The pressure distribution inside the foam domain is presented in Fig. 7a. The effect of a heterogeneous inlet flow has been modeled and shown here. The pressure distribution in Fig. 7a represents the velocity distribution in Fig. 1b. The flow velocity shown in Fig. 1b has an increasing trend at the inlet of the foam from the left to the right side of the inlet. This trend matches with the pressure distribution shown in Fig 7a, which gives a qualitative agreement between the experiment and the simulation results.

Furthermore, from a physical point of view, it is expected that the pressure change from the inlet to the outlet has a

Fig. 7 *Numerical results:* **a** The 2D pressure distribution in the $y-z$ plane at the last time step. **b** The 1D transient pressure distribution at the middle of inlet ($y = 0.5$) in the flow direction

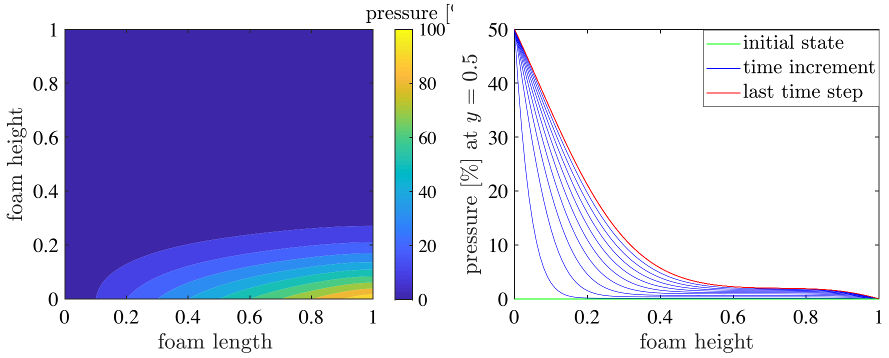

(a)

(b)

semi-linear behaviour. The transient pressure response in the direction of the flow at the middle of the foam at $y = 0.5$ is shown in Fig. 7b. In this figure, the green line is the initial pressure and the red line is the last time step.

4.2.1 Influence of back-coupling calculations

To show the influence of back-coupling calculations, the defined problem is solved once by considering constant values for geometrical parameters (i.e. porosity and permeability) and once by calculating the changes due to coating. The 1D results at the middle of the foam ($y = 0.5$), are presented in Fig. 8 for the ion concentration distribution and radius of struts.

During the deposition process, the coating thickness changes the permeability and porosity which in turn influences the flow behaviour inside the foam. This is the reason for the difference in the magnitudes obtained by the back-coupling calculations in comparison to the magnitudes without the back-coupling calculations in Fig. 8.

4.3 Numerical vs. experimental results: global coating thickness distribution

Figure 9a shows the specific density distribution of the Ni/PU hybrid foam. The range of the density factor varies between 84.2% and 118.1%. The specific density decreases from the edge of the foam plate to the inner center. The distribution of the specific density inside the foam plate seems to be symmetric. The optimized parameter of Kunz et al. [7] can homogenize the deposited mass analyzed by optimized electrolyte flow and anode distance. The analysis along the red, dashed line shows a low density factor in the inner part of the foam, i.e. in the position between 5 and 10 cm, while the outer 5 cm on both sides show a high gradient in the density factor. The inhomogeneities occurring between the outer area of the foam plate and the center cannot be generated by differences in the flow velocity, so they must arise by an inhomogeniously distributed electric field and edge effects, which often occur during electric driven mass transport processes [52].

To obtain a comparable numerical result corresponding to Fig. 9b, the specific density can be associated with the normalized total coating thickness in each specimen. Using the proposed model, the global coating thickness at the y–z plane in the middle of the foam (red, dashed line in Fig. 9a)

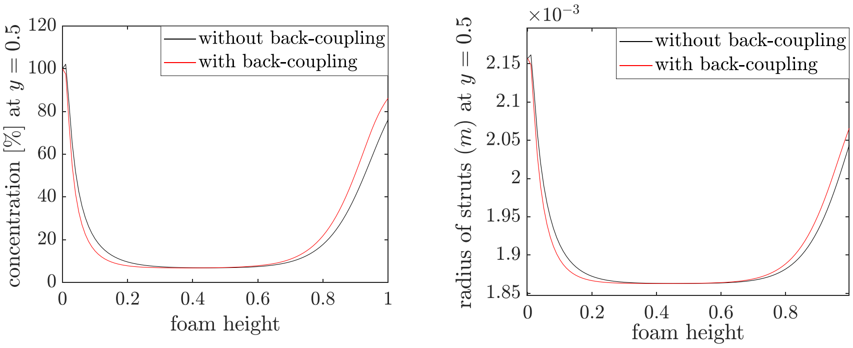

(a)

(b)

Fig. 8 *Numerical results:* The comparison of the **a** concentration distribution and **b** radius of struts, with and without back-coupling calculations, at the middle of inlet ($y = 0.5$) in the flow direction

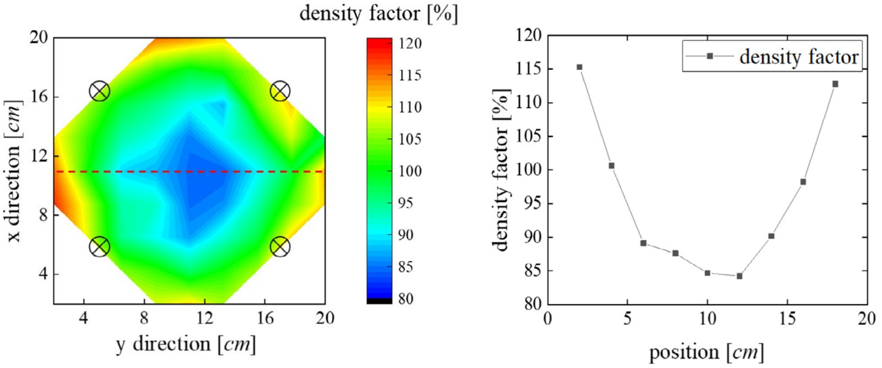

(a)

(b)

Fig. 9 *Experimental results:* **a** Gravimetry plot of the specific density distribution of the cuboid specimens (Fig. 2) taken into account for the analysis in the x–y plane. The crossed circles (⊗) show the inlet points of the current during electrodeposition. The red, dashed line shows the analyzed profile line depicted in (**b**)

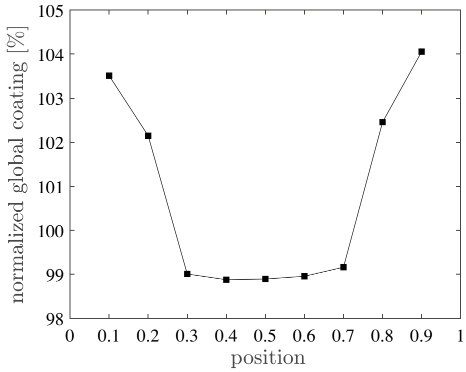

Fig. 10 *Numerical results:* Computed global normalized coating thickness distribution along the red, dashed line shown in Fig. 9a (Color figure online)

is calculated and divided by the average total coating thickness of all specimens. The result is presented in Fig. 10 which shows a similar trend as Fig. 9b, with higher magnitudes at the edges and lower magnitudes in the central parts.

4.4 Numerical vs. experimental results: local and semi-local coating thickness distribution

In this section, the local coating thickness is investigated in three specimens from both sides and from the center of the foam (Fig. 11). The experimental results are compared with the simulation results at the respective positions of the numerical domain.

The averaged, semi-local coating thickness (see Fig. 12a) shows the distribution of the coating thickness in different areas (top, center and bottom) within the foam plate. A simple gravimetric analysis of the density distribution within the foam plane is not sufficient to resolve the gradient of the coating thickness in flow direction. It is also required to analyze the coating along the height of the foam. Starting from the top of the foam, the semi-local coating thickness are the highest with values between 205.5 and 248.7 μm. In the center, the coating thickness at the three prominent locations varies slightly between 58.0 and 64.4 μm. The bottom area of all specimens shows a coating thickness between 126.1 and 202.5 μm, but the bottom area of the cuboid specimen taken out of the center area of the foam plate exhibits the thinnest coating with 126.1 μm. The local coating thickness of the cuboid specimens from the three positions in Fig. 12b shows a similar distribution moving from the outer positions to the inner of the foam. Only the outer regions of the specimens differ. The outer overcoating was discussed in detail in earlier studies [7] and has its origin in the influence of the ad-atom formation at different flow velocities. In general, it can be concluded that the side facing the electrolyte flow shows lower coating thicknesses than the side facing away from the flow. One reason for the higher coating thickness of the top area of the cuboid specimen is also given by gravity. The areas in the middle of the foam plate (10 cm) show

Fig. 11 Schematic description of the cuboid specimens for the local and semi-local analysis

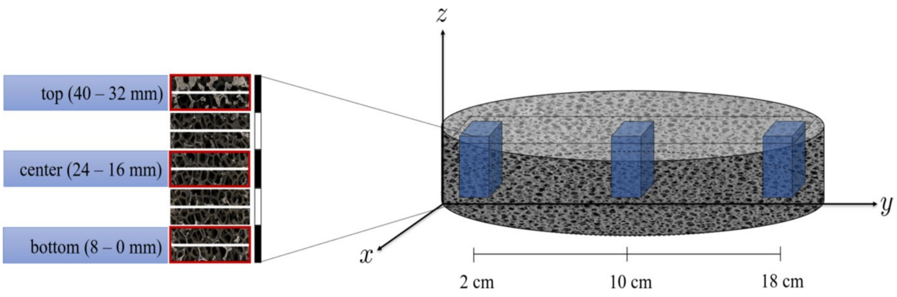

Fig. 12 *Experimental results:* Analysis of three characteristic cuboid specimens from the hybrid foam plate in Fig. 11. **a** Semi-local coating thickness distribution with the averaged thickness values of the top, center and bottom of the cuboid specimen and **b** local coating thickness distribution within each analyzed cuboid specimens

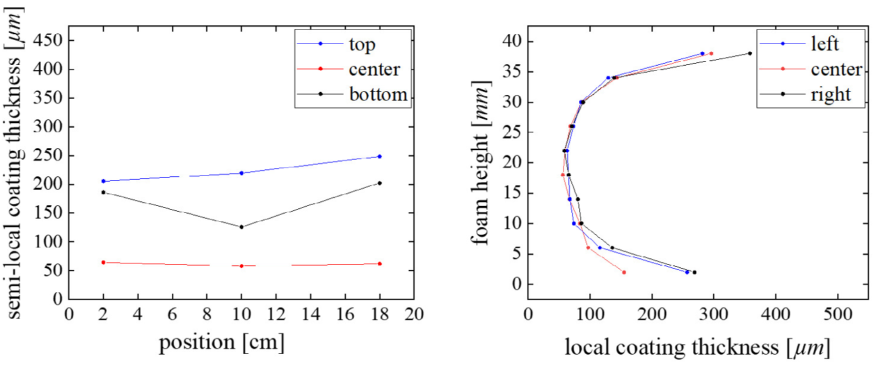

(a) (b)

Fig. 13 *Numerical results:* Numerical simulations of the analysis of three characteristic cuboid specimens shown in Fig. 11. **a** Semi-local coating thickness distribution with the averaged thickness values of the top, center and bottom of the cuboid specimen and **b** local coating thickness distribution within each analyzed cuboid specimens

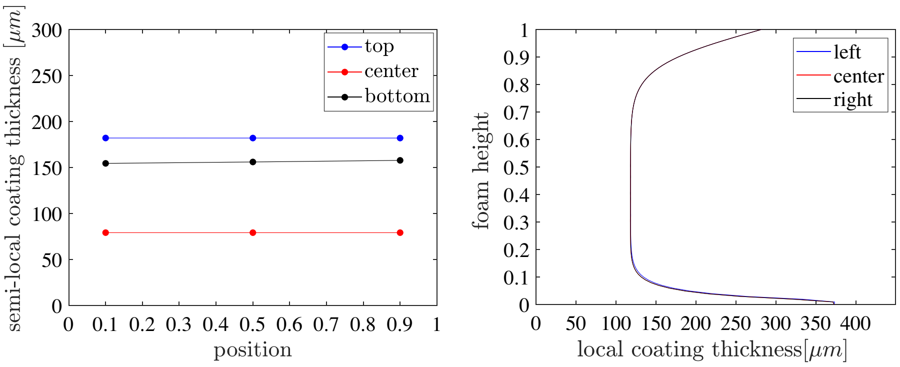

(a) (b)

lower coating thicknesses due to higher resistance of the introduced current by the power supply and lower prevailing electric fields.

Figure 13 depicts the simulation results for the semi-local and local coating distribution in the considered specimens. The trends qualitatively show a good agreement between the model and the experimental results. The coating thickness at the top and bottom is higher than the center of the specimens. Moreover, the semi-local graphs for the top and center parts show approximately constant values for all the specimens in both experimental and simulation results. The quantitative comparison represents a close agreement of the results for the bottom and center, and an offset of 20 μm for the top of the foam. All the three trends in Fig. 13b are overlaying on each other.

The difference in the semi-local results for the bottom of the specimens is due to the definition of the boundary condition at this area. For the sake of simplicity, a constant Dirichlet boundary condition has been defined (see Eq. (19)) and the occurring turbulence at both sides of the inlet near the walls has been neglected. This turbulent flow can affect the distribution of ions at this area and cause a non-homogeneous ion distribution. Hence, the inlet area can be divided into the parts near the walls with high ion concentration and an inner central part with lower concentration levels. Taking into account the approximate values of semi-local coating thickness at the bottom of specimens in Fig. 12a (200 μm at the edges and 140 μm in the middle), it can be concluded that the available ion concentration in the middle part of the boundary is 70 % of the total concentration. Considering the influence of the flow turbulence in the local distribution of ions in the electrolyte, the inlet concentration boundary condition can be modified and assumed as follows:

$$c(y,0,t) = \begin{cases} C_\infty & 0 \le y \le 0.2 \\ 0.7\,C_\infty & 0.2 < y < 0.8 \\ C_\infty & 0.8 \le y \le 1 \end{cases} \tag{35}$$

Moreover, taking a look at Fig. 9a, the local influence of the electrical field at both sides of the foam should also be considered. Therefore, the electrical boundary condition at the inlet and outlet of the foam is not of a homogeneous Dirichlet type; rather, it should be modified as follows:

$$E(y,0,t) = E(y,1,t) = \begin{cases} E_1 & 0 \le y \le 0.2 \\ 0.7\,E_1 & 0.2 < y < 0.8 \\ E_1 & 0.8 \le y \le 1 \end{cases} \tag{36}$$

Fig. 14 *Numerical results:* Using modified boundary conditions in numerical simulations of the microscopic analysis of three characteristic cuboid specimens shown in Fig. 11. **a** Semi-local coating thickness distribution with the averaged thickness values of the top, center and bottom of the cuboid specimen and **b** local coating thickness distribution within each analyzed cuboid specimens

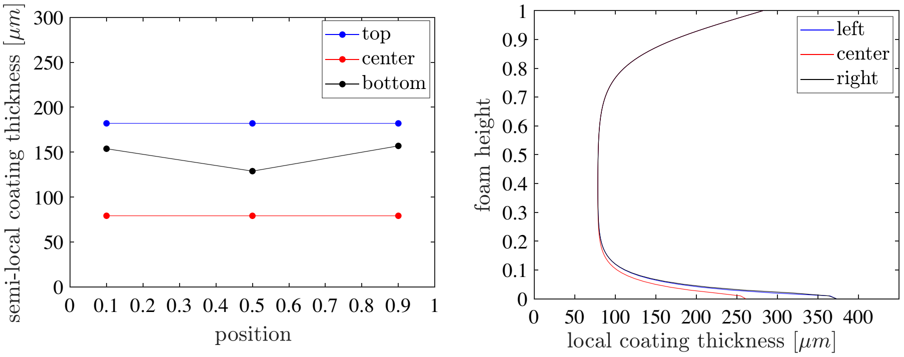

(a) (b)

The simulation results for the modified boundary condition in Eqs. (35) and (36) are shown in Fig. 14. They shows an improved agreement with the experimental results of Fig. 12. The comparison between Figs. 13 and 14 gives an emphasis on the importance of the proper choice of boundary conditions to obtain a more precise simulation.

By comparing Figs. 13 and 14, it can be found from the model that one of the influencing factors on the observed heterogeneous coating thickness is the flow condition and the heterogeneous distribution of ions at the foam inlet. Therefore, to obtain a more homogeneous coating distribution, the ion concentration should be homogeneous as well throughout the inlet boundary.

4.5 Numerical vs. experimental results: investigation of flow

Investigating and understanding the flow behaviour through the open-cell foam assists in understanding its influence on the coating characteristics. It can help to identify the coating-related problems and implement appropriate corrective measures. Figure 15 depicts the components of flow velocity along the inlet of the foam. This estimation has been derived using CFD simulations developed by Autodesk. The input data are based on the conditions and measured parameters in the experiment. Moreover, an .stl file describing the geometry of the foam was used as the input data to compute the internal flow velocity. A detailed description can be found in [7].

Comparing the coating thicknesses, which were measured in the cuboid specimens at defined positions to the simulated flow velocity, it can be concluded, that mainly the upper part of the foam plate is effected by the flow velocity distribution. The coating thickness in the top area increases from 205.5 to 248.7 μm due to higher mass transport of fresh nickel ions through the foam. The two times higher flow velocity at the position 18 cm causes a 21% thicker coating comparing to position 2 cm. The turbulence in this area was given through the deviation of the z-component of the velocity from the dominating absolute velocity.

The proposed model in this study is capable of the calculation of pressure distribution in the domain. According to Darcy's law the velocity is related to the negative pressure gradient ($\mathbf{v} \propto -\mathrm{grad}p$). The negative pressure gradient corresponding to the z- and y-velocity component in the direction of the inlet is shown in Fig. 16. The comparison of the trends in both figures reveals an increase in the z-magnitudes of velocity and accordingly the pressure gradient from the left to the right side of the foam. However, the y-magnitudes of both parameters show similar constant trends.

5 Conclusion

For this work, optimized deposition parameters were used in an electrodeposition process to produce a Ni/PU hybrid foam, which was subsequently characterized in terms of coating thickness distribution. The flow-controlled deposition resulted in excellent homogeneity levels between 85 and 118.1 % even for large samples with a diameter of 210 mm compared to Grill et al. [8]. The distribution of the deposited nickel mass shows a decrease towards the center of the plate. Both in terms of area and volume, the thickness of the coating is higher on the outside than on the inside of the foam. With respect to the thickness of the foam, the coating thickness decreases reciprocally towards the inside of the foam specimen. There is a remaining increase of the coating thickness in the upper as well as in the lower area, which, however, depends on the position in the foam volume and is influenced by gravity, flow velocity, local value of the

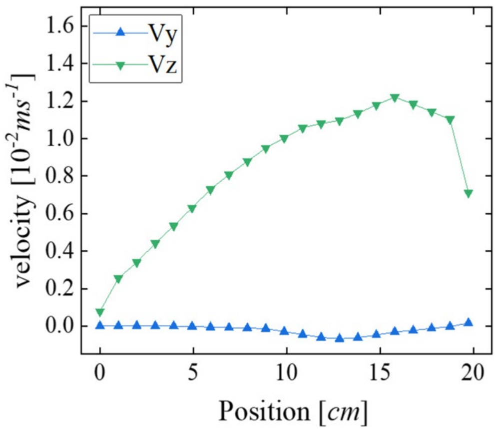

Fig. 15 *Results obtained from experimental input data:* CFD simulation of the electrolyte flow velocity inside the deposition area along (V_z) and across (V_y) the inlet direction

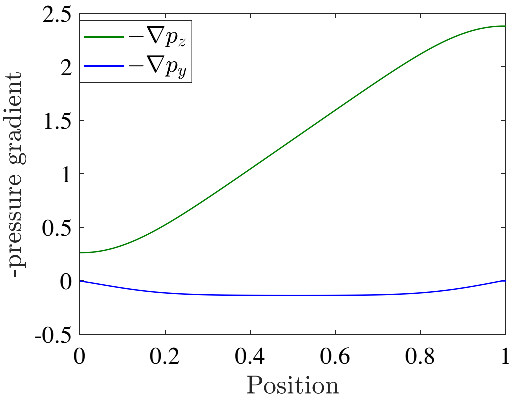

Fig. 16 *Numerical results:* Numerical modelling of the pressure gradient inside the deposition area along (V_z) and across (V_y) the inlet direction

electric field and the conductivity of the dip-coated precursor foam.

A numerical model to describe this electrodeposition process has been proposed. A comprehensive description of the physical process and the experiment's conditions is given. With the help of continuum mixture theory, the process variables and the flow behaviour are accordingly modelled. By taking into account the main transport mechanisms, namely, diffusion, convection and migration, and considering simplified assumptions and defining suitable constitutive equations, the governing system of equations has been derived and solved using Finite Difference Method. The proposed model is capable of dealing with the gradual geometrical changes with deposition and updating the parameters through back-coupling. Different fields, such as transient response of concentration, pressure and electric field distribution, local and global coating thickness and permeability changes can be obtained. The comparison of numerical and experimental results exhibits a strong qualitative correlation and a promising capability of the model to improve the coating process and the homogeneity of coating. The results show that an appropriate choice of boundary conditions is crucial for a qualitatively correct simulation of the experiment. In the current model, due to the lack of information about real boundary conditions, a no flux condition is assumed for the lateral faces of the foam, which led to a 2D simplification. By knowing the exact boundary conditions on the other faces, it can be extended to a 3D model which ultimately leads to more precise results.

Funding Open Access funding enabled and organized by Projekt DEAL. This work was supported by the German Science Foundation (DFG) under the grants DI430/35-1 and JU2962/8-1.

Data availability No datasets were generated or analysed during the current study.

Declarations

Conflict of interest The authors declare no conflict of interest.

References

1. Z. Chen, G. Huan, Y. Ma, *Computational Methods for Multiphase Flows in Porous Media* (SIAM, New Delhi, 2006)
2. M.P. Lautenschlaeger, J. Weinmiller, B. Kellers, T. Danner, A. Latz, Homogenized lattice Boltzmann model for simulating multiphase flows in heterogeneous porous media. Adv. Water Resour. **170**, 104320 (2022)
3. J. Banhart, Manufacture, characterisation and application of cellular metals and metal foams. Prog. Mater Sci. **46**(6), 559–632 (2001)
4. I. Duarte, N. Peixinho, A. Andrade-Campos, R. Valente, Special issue on cellular materials. Sci. Technol. Mater. **30**(1), 1–3 (2018)
5. P.S. Liu, G.F. Chen, *Porous Materials: Processing and Applications* (Elsevier Science, Amsterdam, 2014)
6. A. Jung, S. Diebels, Hybrid metal foams: experimental observations and phenomenological modelling. Techn. Mech. Eur. J. Eng. Mech. **34**(1), 12–22 (2014)
7. F. Kunz, A. Jung, Investigation of the structural coating homogeneity in open-porous nickel/polyurethane hybrid foams produced by flow-controlled electrodeposition. Adv. Eng. Mater. **24**(11), 2200262 (2022)
8. C. Grill, M. Fries, A. Jung, S. Diebels, Numerical and experimental investigations of the electrodeposition process on open porous foams, determination of the parameter influence on the coating homogeneity. Int. J. Heat Mass Transf. **180**, 121791 (2021)
9. A. Jung, M.R. Koblischka, E. Lach, S. Diebels, H. Natter, Hybrid metal foams: mechanical testing and determination of mass flow limitations during electroplating. Int. J. Mater. Sci. **2**(1), 97–107 (2012)
10. A. Jung, S. Diebels, Synthesis and mechanical properties of novel Ni/PU hybrid foams: a new economic composite material for energy absorbers. Adv. Eng. Mater. **18**(4), 532–541 (2016)
11. A. Jung, H. Natter, S. Diebels, E. Lach, R. Hempelmann, Nanonickel coated aluminum foam for enhanced impact energy absorption. Adv. Eng. Mater. **13**(1–2), 23–28 (2011)
12. A. Jung, S. Diebels, Micromechanical characterization of metal foams. Adv. Eng. Mater. **21**(8), 1900237 (2019)
13. B. Bouwhuis, J. McCrea, G. Palumbo, G. Hibbard, Mechanical properties of hybrid nanocrystalline metal foams. Acta Mater. **57**(14), 4046–4053 (2009)
14. Y. Boonyongmaneerat, C.A. Schuh, D.C. Dunand, Mechanical properties of reticulated aluminum foams with electrodeposited ni-w coatings. Scr. Mater. **59**(3), 336–339 (2008)
15. Y. Sun, R. Burgueño, A.J. Vanderklok, S.A. Tekalur, W. Wang, I. Lee, Compressive behavior of aluminum/copper hybrid foams under high strain rate loading. Mater. Sci. Eng. A **592**, 111–120 (2014)
16. Y. Sun, R. Burgueño, W. Wang, I. Lee, Effect of annealing on the mechanical properties of nano-copper reinforced open-cell aluminum foams. Mater. Sci. Eng., A **613**, 340–351 (2014)
17. Y. Sun, R. Burgueño, W. Wang, I. Lee, Modeling and simulation of the quasi-static compressive behavior of al/cu hybrid open-cell foams. Int. J. Solids Struct. **54**, 135–146 (2015)
18. K.J. Euler, Die änderung der stromverteilung in porösen positiven elektroden von akkumulatoren und galvanischen primärzellen während ladung und entladung. Electrochim. Acta **13**(7), 1533–1549 (1968)
19. K.J. Euler, Stromverteilung in und auf porösen elektroden. Chem. Ing. Tecn. **37**(6), 626–631 (1965)
20. K.J. Euler, Spatial current distribution in non-isotropic conductors (with implication for porous electrodes). Electrochim. Acta **18**(5), 385–387 (1973)

21. N. Ghiasi, A. Jung, S. Diebels, Modelling the electrodeposition of nickel on polyurethane foam. Contin. Mech. Thermodyn. (submitted) (2023)
22. R.M. Bowen, R.A. Grot, G.A. Maugin, *Continuum Physics, Volume III: Mixtures and EM Field Theories* (Academic Press, New York, San Francisco, London, 1976)
23. W. Ehlers, J. Bluhm, *Porous Media: Theory, Experiments and Numerical Applications* (Springer, Berlin, 2002)
24. C. Truesdell, R. Toupin, The classical field theories, in *Principles of Classical Mechanics and Field theory/Prinzipien der Klassischen Mechanik und Feldtheorie*. ed. by S. Flügge (Springer, New York, 1960), pp.226–858
25. P. Sharma, S. Diebels, A mixture theory for the moisture transport in polyamide. Continuum Mech. Thermodyn. **33**(4), 1891–1905 (2021)
26. M. Manninen, V. Taivassalo, S. Kallio, *On the Mixture Model for Multiphase Flow* (VTT Publications, Finland, 1996)
27. H. Kai, J. Ari, K. Sirpa, K. Hannu, K. Markku, K. Antti, M. Mikko, T. Veikko, *Multiphase Flow Dynamics Theory and Numerics*, vol. 3 (VTT Technical Research Centre of Finland, Vuorimiehentie, Finland, 2009)
28. T. Ricken, A. Schwarz, J. Bluhm, A triphasic theory for growth in biological tissue-basics and applications. Mater. Werkstofftechn. Entwickl. Fertig. Prüf. Eigensch. Anwen. Techn. Werkstoffe **37**(6), 446–456 (2006)
29. G. Del Bufalo, L. Placidi, M. Porfiri, A mixture theory framework for modeling the mechanical actuation of ionic polymer metal composites. Smart Mater. Struct. **17**(4), 045010 (2008)
30. S. Diebels, Mikropolare zweiphasenmodelle: Modellierung auf der basis der theorie poröser medien (2000)
31. S. Diebels, A micropolar theory of porous media: constitutive modelling. Transp. Porous Media **34**, 193–208 (1999)
32. C. Grill, A. Jung, S. Diebels, Modelling and simulation of the coating process on open porous metal foams. PAMM **18**(1), 201800254 (2018)
33. C. Grill, A. Jung, S. Diebels, Investigation of the electrodeposition parameters on the coating process on open porous media. PAMM **19**(1), 201900106 (2019)
34. J. Kauffman, J. Gilbert, E. Paterson, Multi-physics modeling of electrochemical deposition. Fluids **5**(4), 240 (2020)
35. D. Noren, M.A. Hoffman, Clarifying the Butler–Volmer equation and related approximations for calculating activation losses in solid oxide fuel cell models. J. Power Sources **152**, 175–181 (2005)
36. E.J. Dickinson, A.J. Wain, The Butler–Volmer equation in electrochemical theory: origins, value, and practical application. J. Electroanal. Chem. **872**, 114145 (2020)
37. M. Kamata, M. Paku, Exploring Faraday's law of electrolysis using zinc-air batteries with current regulative diodes. J. Chem. Educ. **84**(4), 674 (2007)
38. S. Diebels, *Micropolar Mixture Models on the Basis of the Theory of Porous Media* (Springer, Berlin, 2002)
39. M. Miyan, P.K. Pant, Flow and diffusion equations for fluid flow in porous rocks for the multiphase flow phenomena. Am. J. Eng. Res. (AJER) **4**(7), 139–148 (2015)
40. J.I. Siddique, A. Ahmed, A. Aziz, C.M. Khalique, A review of mixture theory for deformable porous media and applications. Appl. Sci. **7**(9), 917 (2017)
41. W.B. Fulks, R.B. Guenther, E.L. Roetman, Equations of motion and continuity for fluid flow in a porous medium. Acta Mech. **12**(1), 121–129 (1971)
42. J.J. Jasielec, Electrodiffusion phenomena in neuroscience and the Nernst–Planck–Poisson equations. Electrochemistry **2**(2), 197–215 (2021)
43. H. Cohen, J.W. Cooley, The numerical solution of the time-dependent Nernst–Planck equations. Biophys. J . **5**(2), 145–162 (1965)
44. A. Mahapatro, S.K. Suggu, Modeling and simulation of electrodeposition: effect of electrolyte current density and conductivity on electroplating thickness. Adv. Mater. Sci. **3**(2), 1 (2018)
45. J. Newman, N.P. Balsara, *Electrochemical Systems* (John Wiley & Sons, New York, 2021)
46. J. Hommel, E. Coltman, H. Class, Porosity-permeability relations for evolving pore space: a review with a focus on (bio-) geochemically altered porous media. Transp. Porous Media **124**(2), 589–629 (2018)
47. Z. Li, Z. Qiao, T. Tang, *Numerical Solution of Differential Equations: Introduction to Finite Difference and Finite Element Methods* (Cambridge University Press, Cambridge, 2017)
48. M.H. Holmes, *Introduction to Numerical Methods in Differential Equations* (Springer, Berlin, 2007)
49. R.J. LeVeque, Finite difference methods for differential equations. Draft version for use in AMath vol. **585**(6), p. 112 (1998)
50. W.F. Ames, *Numerical Methods for Partial Differential Equations* (Academic press, USA, 2014)
51. H. Sato, M. Yui, H. Yoshikawa, Ionic diffusion coefficients of cs+, pb2+, sm3+, ni2+, seo2-4 and tco- 4 in free water determined from conductivity measurements. J. Nucl. Sci. Technol. **33**(12), 950–955 (1996)
52. T. Pérez, L.F. Arenas, D. Villalobos-Lara, N. Zhou, S. Wang, F.C. Walsh, J.L. Nava, C.P. de León, Simulations of fluid flow, mass transport and current distribution in a parallel plate flow cell during nickel electrodeposition. J. Electroanal. Chem. **873**, 114359 (2020)